# Synthesis and characterization of biodegradable lignin nanoparticles with tunable surface properties

Alexander P. Richter[1,2], Bhuvnesh Bharti[1], Hinton B. Armstrong[1,2], Joseph S. Brown[1], Dayne Plemmons[1], Vesselin N. Paunov[3], Simeon D. Stoyanov[4,5] and Orlin D. Velev[1*]

[1] Department of Chemical and Biomolecular Engineering North Carolina State University, Raleigh, NC 27695, USA

[2] BENANOVA Inc., Raleigh, NC 27606, USA

[3] Department of Chemistry, University of Hull, Hull, HU67RX, UK

[4] Physical Chemistry and Soft Matter, Wageningen University, Wageningen, The Netherlands

[5] Department of Mechanical Engineering, University College London, Torrington Place, London, WC1E 7JE, UK

Revised manuscript submitted to *Langmuir*, June 2, 2016

**ABSTRACT:** Lignin nanoparticles can serve as biodegradable carriers of biocidal actives with minimal environmental footprint. Here we describe the colloidal synthesis and interfacial design of nanoparticles with tunable surface properties using two different lignin precursors, Kraft (Indulin AT) lignin and Organosolv (High Purity Lignin). The green synthesis process is based on flash-precipitation of dissolved lignin polymer, which enabled the formation of nanoparticles in the size range of 45 to 250 nm. The size evolution of the two types of lignin particles is fitted on the basis of modified diffusive growth kinetics and mass-balance dependencies. The surface properties of the nanoparticles are fine-tuned by coating them with a cationic polyelectrolyte, polydiallyldimethylammonium chloride. We analyze how the colloidal stability and dispersion properties of these two types of nanoparticles vary as a function of pH and salinities. The data show that the properties of the nanoparticles are governed by the type of lignin used and the presence of polyelectrolyte surface coating. The coating allows the control of the nanoparticles' surface charge and the extension of their stability into strongly basic regimes, facilitating their potential application at extreme pH conditions.

## 1. INTRODUCTION

Engineered nanomaterials have the potential to solve challenges in the fields of environmental remediation,[1] food and agriculture,[2] and health care.[3] However, the possible risk associated with the use of many synthetic inorganic nanoparticles and their post-utilization activity have limited their large scale application.[4] The deactivation of waste nanoparticles in solid-waste incineration plants,[5] or the recovery of persistent nanoparticles in wastewater treatment systems,[6] is a non-trivial problem. The potential post-utilization activity of such nanoparticles[7] combined with their possible persistence,[5,8] could lead to long-term environmental impact.[9] It has been demonstrated previously that by applying green chemistry principles[10] at the early stage of nanomaterial engineering one can solve or mitigate some of these problems,[11] and synthesize sustainable functional nanomaterials.[12]

Biodegradable nanoparticles prepared from renewable feedstock could be used for safer delivery of active ingredients in molecular or ionic form.[13,14] After cellulose, lignin is the second most abundant biopolymer in nature and the first most abundant aromatic one.[15,16] It has an amorphous structure,[17] where the polymeric building block units form a three-dimensional network.[18] Lignin is an antioxidant[19] and lacks cytotoxicity towards human cells.[20,21] Since lignin is of plant origin,[22] it is naturally degradable and biocompatible.[23] Microbial decomposition of lignin in the environment[24] transforms it to form the bulk component of soil humus or natural compost.[25] This biodegradability of lignin makes it an ideal precursor for developing environmentally friendly nanoscale materials. The most common industrial-scale method to extract lignin is the Kraft pulping process[26] from which alkali lignin, such as Indulin AT lignin from MeadWestvaco Corp. is recovered. This lignin contains several hydrophilic functional groups such as carboxylic, phenolic and aliphatic hydroxyl groups as well as a small number of thiol groups, whose relative fractions are listed in Table 1.[27] These functional groups have chelating properties towards metallic micronutrients, e.g. Fe, Zn, and Mn. Due to the environmentally sustainable nature of lignin,[28] it has been used for the delivery of such micronutrients in agronomic products.[29,30] Lignin obtained via the Organosolv process, such as High Purity Lignin (HPL) from Lignol Innovations Ltd. is highly hydrophobic (see solvent properties in Table S2) and classified as sulfur-free.[15,27]

Lignin nanoparticles have been previously synthesized by precipitation methods initiated with acids,[31,32] $CO_2$ saturation,[33] continuous solvent exchange,[34] and dialysis,[35] as well as by sonication[36] and other water-in-oil micro emulsion based methods.[37,38] The physical properties of these particles such as hydrophobicity, surface charge, and stability are dependent on the type of lignin precursor and the nanoparticle synthesis technique. This wide variation of the surface properties of the lignin nanoparticles makes them suitable for controlled functionalization with actives for environmental-friendly applications. Recently, we showed that green chemistry principles[10,12,31] can be applied to synthesize environmentally-benign antimicrobial nanoparticles from lignin cores infused with silver ions.[39] The targeting efficiency of

the nanoparticles towards negatively-charged bacterial cell membranes was enabled by reversal of their surface charge. The charge inversion from negative to positive was achieved by the adsorption of a cationic polyelectrolyte, polydiallyldimethylammonium chloride (PDAC). These biodegradable nanoparticles have shown broad-spectrum antimicrobial activity, and their extensive toxicity evaluation by the EPA ToxCast™ program suggests that they are environmentally friendly alternative to more persistent metallic silver nanoparticles.[39]

The objectives of this study are to develop new strategies to synthesize lignin nanoparticles with surface functionalities enabling their use as nanocarriers for a broad spectrum of ionic and hydrophobic active ingredients. We report the synthesis of two types of lignin nanoparticles of different precursors, namely (a) Indulin AT and (b) HPL, using flash-precipitation methods.[40] Nanoparticles made of Indulin AT are partly hydrophilic, and hence are suitable for functionalization with ionic active ingredients, such as antimicrobial silver ions.[39] The lignin nanoparticles from HPL are highly hydrophobic, and a suitable carrier for hydrophobic actives, such as organic fungicides in crop-protection.

The paper is organized as follows: First, we will present details on the pH induced flash-precipitation of Indulin AT lignin nanoparticles in ethylene glycol and investigate their growth mechanism. The surface charge inversion and stability studies of native and PDAC-coated particles were performed using light scattering and zeta potential measurements. In the second part of the paper, we present a new synthetic approach for the synthesis of nanoparticles made of HPL. In this case, the flash-precipitation was induced by addition of antisolvent to super-saturate the dissolved lignin in acetone solution. The surface properties of native and PDAC-coated HPL nanoparticles were also investigated. At the end, we compare the colloidal properties of both types of nanoparticles and highlight some of their similarities and differences.

**Table 1.** Functional groups of High Purity Lignin and Indulin AT lignin. Types of main functional groups and their occurrence per one hundred aromatic rings according to literature data from MeadWestvaco Corp. and Lignol Innovations Ltd. The approximate pKa values of the corresponding functional groups are reported.

| **Functional group** | **High Purity Lignin (per 100 aromatic rings)** | **Indulin AT (per 100 aromatic rings)** | **pKa** |
|---|---|---|---|
| Phenolic OH | 73 | 68 | 10 (Ref. [41]) |
| Aliphatic alcohol | 34 | 51 | 16-17 (Ref. [42]) |
| Thiol | n/a | 9 | 10-11 (Ref. [42]) |
| Carboxylic acid | n/a | 16 | 4.2 (Ref. [43]) |

## 2. EXPERIMENTAL SECTION

**Materials.** Kraft lignin, Indulin AT lignin powder (lot # MB05) was obtained from MeadWestvaco (MWV) Corp., USA. Organosolv lignin, High Purity Lignin (HPL) powder with number average molecular weight of 969 Da, was obtained from Lignol Innovations Ltd., CA. Ethylene glycol (purity > 99 %), nitric acid, polydiallyldimethylammonium chloride (PDAC) with a molecular weight of 100,000 – 200,000 was obtained from Sigma Aldrich, USA. Acetone (purity > 99.5 %), sodium hydroxide, Whatman Anotop 25 - 0.02 μm and 0.45 μm nylon syringe filters were obtained from Fisher Scientific, USA. Dialyzed water was prepared with a Millipore RiOS™ system combined with a Synergy UV module.

**Synthesis of Indulin AT nanoparticles.** In a typical batch synthesis of the nanoparticles, 0.25 g of Indulin AT biopolymer was dissolved in 50 mL ethylene glycol. The solution was vortexed for 30 minutes, filtered with a 0.45 μm syringe filter, and placed into a scintillation vial. The particles were synthesized by rapidly adding 1.0 to 3.0 mL of 0.025 M $HNO_3$ to 5 mL of ethylene glycol containing dissolved lignin, while vigorously stirring the sample. For the particle growth study in ethylene glycol (Figure 2a), 1.375 mL of 0.025 M $HNO_3$ was added to 5 mL of lignin solution. The particle growth was monitored over time by measuring the hydrodynamic diameter of the particles using DLS.

**Synthesis of HPL nanoparticles.** In a typical Organosolv lignin nanoparticle batch synthesis, 0.25 g of High Purity Lignin was dissolved in 50 mL acetone. The stock solution was vortexed for 30 minutes and filtered with a 0.45 μm syringe filter. Then, 1 mL of the solution was placed into a 20 mL scintillation vial. Addition of 9.2 mL of water induced super-saturation of lignin in the solution, and resulted into phase separation of lignin in the form of nanoparticles. The samples obtained were then further diluted with water to 0.05 wt %, which provided a suitable concentration for size measurements with DLS.

**Control of antisolvent addition rate for HPL nanoparticle synthesis.** In a typical experiment, 1 mL of 0.5 wt % HPL lignin in acetone was transferred into a glass vial. In the second step, 9.2 mL of the antisolvent, water, was added to the vial. A syringe pump was used to control the rate of antisolvent addition in the range of 1 to 220 mL/min. Further increase in antisolvent addition rate (up to 1100 mL/min) was achieved by direct pipetting.

**HPL nanoparticle sample preparation for ionic strength study**. The particles were synthesized by the procedure presented in the previous section. The salinity study was performed in purely aqueous dispersions and hence, after HPL nanoparticles synthesis, residual acetone was removed via dialysis. The particle suspension was further diluted to 0.05 wt % HPL nanoparticle content at pH 4.5. The pH of the dispersion was adjusted by adding minimum amounts of 1M $HNO_3$ and 1M NaOH solution. The samples were balanced with water to obtain a constant HPL wt % in all measurement samples.

**Dynamic Light Scattering.** A Zetasizer Nano ZSP (Malvern Instruments Ltd.) was used for nanoparticle size measurements. The instrument was fitted with a 633 nm He-Ne laser. The measurements

were performed at 173° in the back-scattering mode. Further details on the measurement procedures and instrument settings are provided in supplementary information (see page S2).

**Zeta potential.** A dip-cell (Malvern, ZEN1002; 2 mm gap size between the electrodes) combined with a 13° forward scatter detector was utilized for measuring the zeta potential of nanoparticles. A voltage of ≤ 5 V was applied.

**Transmission Electron Microscopy.** A JEOL 2000-FX Intermediate Voltage Scanning Transmission Electron Microscope at 200.0 kV excitation voltage was employed for imaging of HPL nanoparticles. For sample preparation, 5 µl droplet of dilute nanoparticle solution was pipetted on a copper TEM grid. After 30 seconds of contact time, the residual volume of the nanoparticle solution was removed by gently blotting with a Kimwipe®. The samples were kept stored in a TEM grid box until analysis.

**Ultraviolet-visible spectroscopy (UV-Vis).** A Jasco V-550 UV-Vis spectrometer was utilized for absorbance measurement at 285 nm to determine the amount of dissolved lignin in aqueous solution and in ethylene glycol. The UV-Vis calibration curves for dissolved Indulin AT lignin in water and ethylene glycol are shown in Figure S1 and S2 respectively.

## 3. RESULTS AND DISCUSSION

**Indulin AT Lignin Nanoparticles - Synthesis of Indulin AT Lignin Nanoparticles.** The first type of nanoparticles investigated were synthesized from Indulin AT lignin. We used a pH drop induced flash-precipitation in ethylene glycol solution to synthesize the nanoparticles.[31,39,44] Figure 1 illustrates the particle synthesis method, in which the pH drop in ethylene glycol triggers supersaturation of Indulin AT, followed by nucleation and particle growth. The parameters controlling the particle size are (a) the initial lignin concentration, (b) the molarity of the acid added, and (c) the rate of acid addition.[31] We investigated the particle growth at rapid acid addition,[31] which relates to instantaneous mixing and pH drop in ethylene glycol (for details see Experimental Section). The particles were diluted with water to cease further increase in size and were then characterized for their colloidal stability and surface properties.

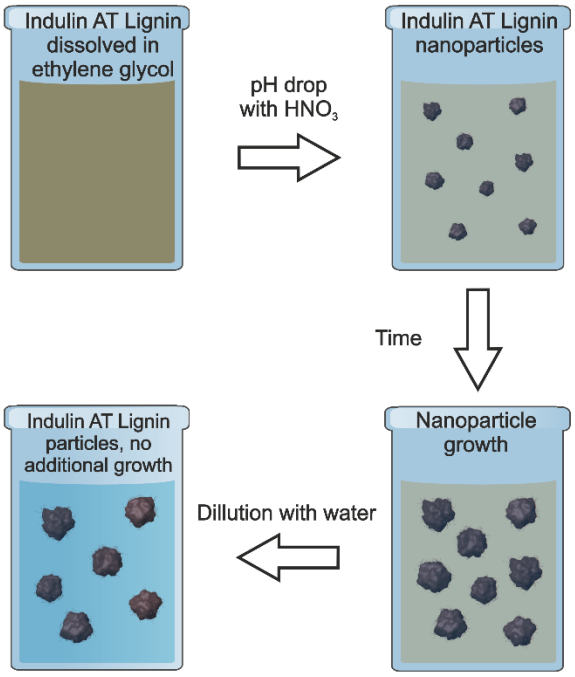


**Figure 1**. Scheme of the synthesis and growth of Indulin AT lignin nanoparticles. The Indulin AT polymer is dissolved in ethylene glycol, in which particles are formed after an induced pH drop. The temperature-dependent particle growth can be ceased by dilution with water.

**Growth kinetics of Indulin AT Nanoparticles**. The nuclei formed during the rapidly induced initial pH drop grow gradually over time, which allows to attain the target nanoparticle size. The change in the size of Indulin AT lignin nanoparticles in ethylene glycol after the initial pH drop (Figure 1) was monitored using Dynamic Light Scattering (DLS). The data for the increase in hydrodynamic diameter ($D_{IAT}$) of the particles as a function of time, $t$, at temperature, $T$ = 25 °C, are plotted in Figure 2a. In general, the kinetics of nanoparticle/nanocrystal growth shows an exponential increase as[45,46]

$$D \propto t^{1/x} \qquad (1)$$

where $D$ is the diameter of the particle at time $t$, and the exponential coefficient $x$ depends on the limiting step of the particle growth mechanism. In our case of lignin nanoparticles at 25°C, we find $x \approx 8$ (Figure 2a). This exponential increase in the particle diameter is much slower than diffusion limited ($x$ = 3) or surface reaction limited ($x$ = 2) particle growth predictions of the common Lifshitz-Slyozov-Wagner (LSW) model.[47] In our case of lignin nanoparticles, the retarded particle growth with $x$ = 8 is similar to the one previously observed for the diffusion-limited growth of silver nanocrystals.[48] For the lignin nanoparticles, the decrease in the exponent of the power law scaling can be attributed to the capping of the lignin nanoparticles with higher molecular weight lignin monomers/impurities present in the solution,[49] and the progressive reduction in the effective concentration of dissolved lignin over time.

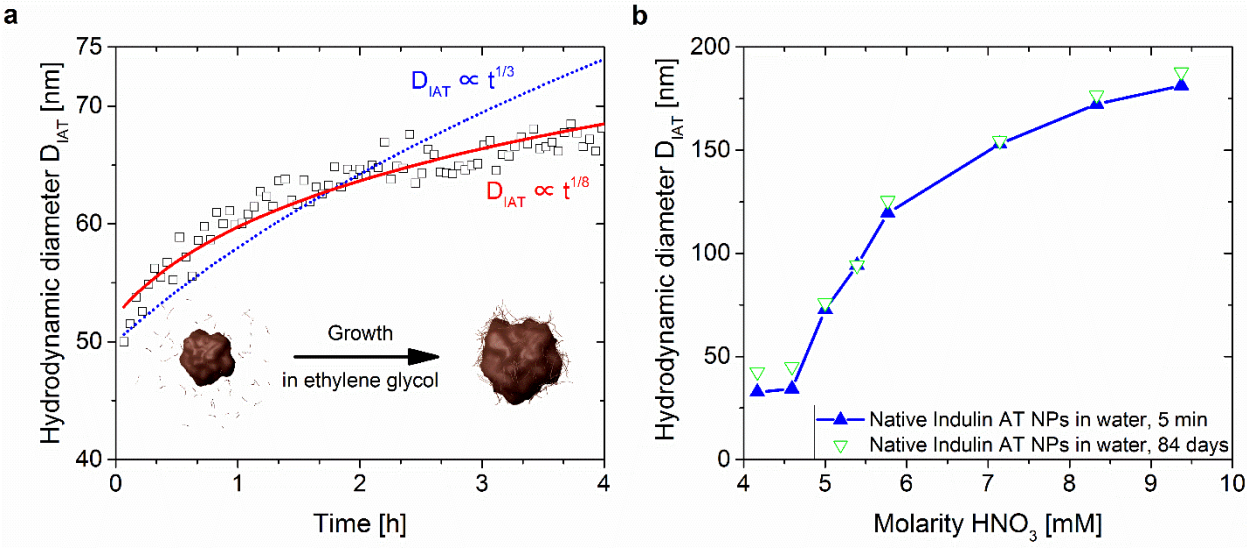


**Figure 2.** Methodology for size control of Indulin AT nanoparticle. **a,** Increase in particle diameter after initial pH drop induced with $HNO_3$ addition (5 mM final concentration) in ethylene glycol containing dissolved lignin as a function of time. The change in particle size shows $D_{IAT} \propto t^{1/8}$ dependence. **b,** Particle diameters as a function of initial $HNO_3$ added, reported as final molarity in solution after pH drop. Here, the nanoparticle dispersions were diluted using DI water after 30 seconds of particle growth in ethylene glycol. The nanoparticles remain stable in size when stored in water containing residual amounts of ethylene glycol, as confirmed by measurements obtained after as long as 84 days. Experimental results reported in **a** are from a single data set. Error bars in **b** represent the standard deviation of experimental values and are less than the symbol size used.

In addition to experiments at $T = 25$ °C, we investigated the particle growth at 35, 38, and 50 °C (Figure S3). At all these temperatures, we observe $x \geq 8$. The average particle diameter increases with increasing temperature from 25 to 50 °C. This increase in size could be attributed to the increased solubility and larger rate of polymer self-diffusion at higher temperatures.[50] The time-dependent particle growth has also been confirmed by measuring the decrease in free lignin content in the supernatant (Figure S4). The increase in the particle diameter ceased upon exchanging the dispersion medium (ethylene glycol) with water (Figure S5). This provides good control over the particle size, where the growth can be stopped by changing the solvent from ethylene glycol to water.

The nanoparticle formation can be initiated by the addition of a strong acid to a solution of lignin dissolved in ethylene glycol. In the present study we use nitric acid ($HNO_3$) for inducing instantaneous pH drop.[39] The amount of acid added determines the relative population of nuclei formed and their growth rate.

The change in nanoparticle diameters with increasing amounts of $HNO_3$ added is shown in Figure 2b and S6. Here, the particles were transferred into water within 5 min of initial growth in ethylene glycol.

**Properties of Indulin AT Nanoparticles**. The as-synthesized Indulin AT lignin nanoparticles, hereafter called *native* nanoparticles, were stable in aqueous dispersion. This colloidal stability can be attributed to the electrostatic repulsion induced by the high negative surface charge of the particles (Figure 3a). Some applications of these nanoparticles, such as targeted microbicide delivery systems, require their surfaces to be positively charged.[39] This charge inversion can be achieved by the adsorption of cationic polyelectrolyte, e.g. PDAC, onto the surface of the nanoparticles. The data for the change in the surface charge of the particles upon the PDAC adsorption, and their corresponding zeta potential are plotted in Figure 3a. Native nanoparticles exhibited a negative zeta potential at all pH values, while PDAC-coated nanoparticles had an isoelectric point at pH 11, below which they were positively charged. The measured sizes of native nanoparticles and PDAC-coated nanoparticles as a function of pH are shown in Figure 3b. The loss of colloidal stability in these samples is indicated by particle size increase upon aggregation and decrease upon dissolution. Both native and PDAC-coated particles exhibit in-solution stability down to pH 2, and show signs of aggregation at pH < 2. This aggregation of native and the PDAC-coated Indulin AT nanoparticles at low pH can be correlated to the observed decrease in the magnitude of the zeta potential below |± 20 mV| for each system, indicating weak electrostatic repulsion between the particles. The PDAC-coated nanoparticle dispersions at pH > 10.5 showed aggregation due to loss of electrostatic stabilization. The corresponding zeta potential decreased below +10 mV, which is close to the charge-neutral point. This behavior of the PDAC-coated particles may be attributed to the increased propensity for dissolution of the biopolymer driven by increased polarity of lignin.[51] The release of negatively charged lignin molecules from within the interior of the nanoparticles, could diminish the cationic charge excess from PDAC by the re-configurations and complexation of the PDAC with the anionic lignin molecules.

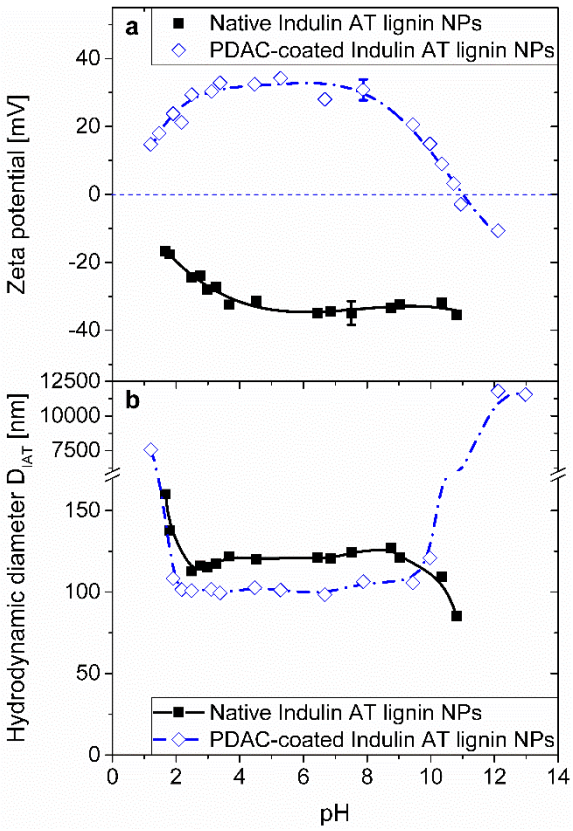


**Figure 3.** Surface charge related properties of Indulin AT lignin nanoparticles. **a,** Zeta potential of native and PDAC-coated nanoparticles as a function of pH. Native nanoparticles exhibit negative zeta potentials at all pH values, while the PDAC-coated nanoparticles exhibit positive zeta potentials up to its isoelectric point at pH 11, above which the particles exhibit a negative zeta potential as well. **b,** Diameter of native and PDAC-coated nanoparticles as a function of pH. Native and PDAC-coated nanoparticles aggregate at pH < 2, as indicated by increasing diameters. PDAC coated nanoparticles aggregate at pH > 10.5, while native nanoparticles show signs of dissolution as indicated by decreasing diameters. Error bars in **a** represent the standard deviation of experimental values, and the bars in **b** for samples below 300 nm in diameter are less than the symbol size used.

The stability of Indulin AT nanoparticles was further investigated by measuring and analyzing the percentage of lignin in particulate and molecularly dissolved form at different pH values by UV-Vis spectrophotometry (Experimental Section). The mass percentage of Indulin AT in nanoparticle form as a function of pH is plotted in Figure 4a. Native Indulin AT nanoparticles progressively dissolve with increasing pH value, while the PDAC-coated particles do not. For native Indulin AT nanoparticles, > 50 % of lignin remained in particulate form at pH 8.2. The particles exhibited nearly complete dissolution at pH > 10.7 with < 4 % of lignin remaining in particulate form, which is in agreement with the known pH dependent solubility properties of Indulin AT.[31] However, for PDAC-coated Indulin AT nanoparticles at pH > 10.7, we find > 90 % of lignin remaining in particulate/aggregate form (Figure 4b, 3b). At low pH values, the net

charge on the native lignin particle decreases significantly and leads to the particle aggregation. In the case of PDAC-coated nanoparticles, a reduction in the pH leads to a decrease in the surface charge density on the lignin core. This decrease in the surface charge sites on lignin would result into a reduced electrostatic attraction between the particle surface and adsorbed PDAC molecules, leading to the partial desorption of the PDAC from the nanoparticle surface. Similar effects have been observed for pH-induced sorption of PDAC on charged surfaces.[52] Desorption of the polyelectrolyte renders the particle cores electrostatically unstable and drives the observed aggregation (Figure 3b). At elevated pH, only the native Indulin AT nanoparticles dissolved due to mutual repulsions between individual polymer strands forming the particles, while the PDAC-coated nanoparticles aggregated due to loss of electrostatic stabilization. In summary, both dispersions were stable in a broad pH regime ranging from pH 2 to 8.2 for native and pH 2 to 10 for PDAC-coated particles.

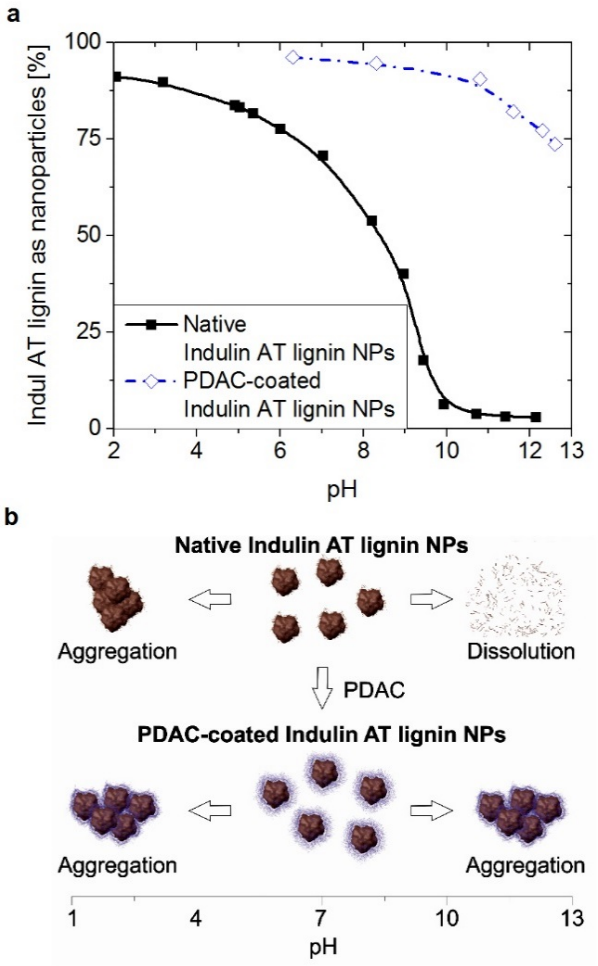


**Figure 4.** Indulin AT lignin nanoparticle aggregation and dissolution. **a,** Percentage of lignin present in particulate form as a function of pH value for native and PDAC coated nanoparticles. **b,** Schematic representation of the pH dependent physical state of native and PDAC-coated nanoparticles in pH range from 1 to 13. At pH < 2, aggregation

was observed for both native and PDAC-coated particles. With increasing pH value, the native nanoparticles dissolve, while in contrast the PDAC-coated nanoparticles aggregate.

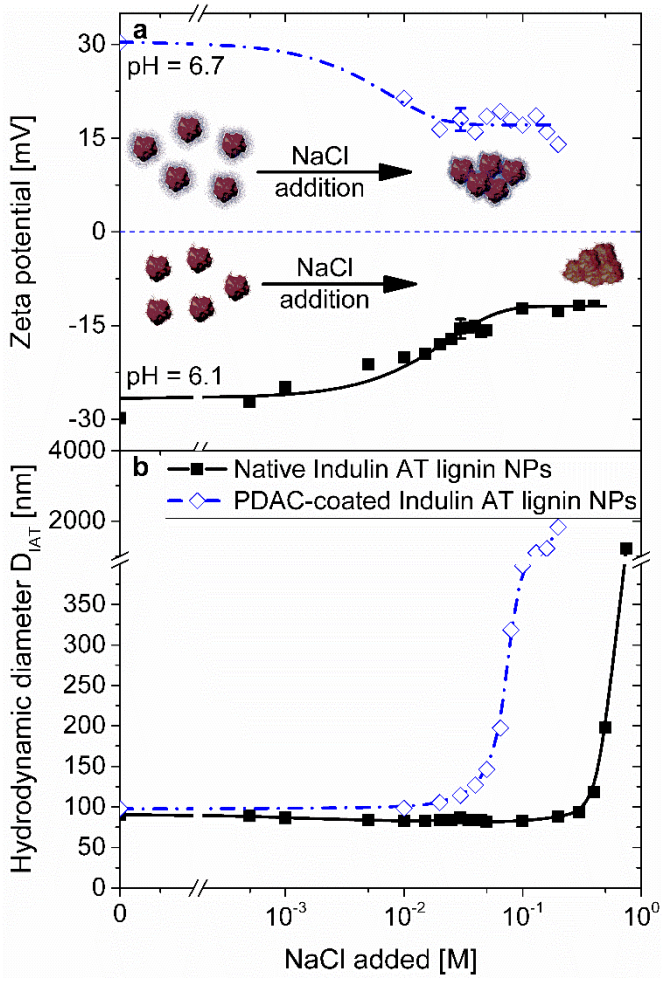


**Figure 5**. Ionic strength stability of Indulin AT lignin nanoparticles. **a,** Zeta potential of native and PDAC-coated nanoparticles as a function of NaCl added. Both nanoparticle systems exhibit colloidal stability at zeta potential magnitudes of 20-30 mV. The native nanoparticles retain their colloidal stability up to 300 mM NaCl added. **b,** Diameter of native and PDAC-coated nanoparticles as a function of NaCl added in final sample. The PDAC-coated nanoparticles aggregate at lower molarity of NaCl. Error bars in **a** represent the standard deviation of experimental values, and the bars in **b** for samples below 300 nm in diameter are less than the symbol size used.

We investigated the effect of the ionic strength on the stability of native and PDAC-coated Indulin AT nanoparticles. The native nanoparticles were dialyzed with water to remove residual ethylene glycol. The ionic strength in the samples was adjusted by the addition of 1:1 electrolyte, NaCl. The zeta potentials of native nanoparticles at pH ~ 6.1 and PDAC-coated particles at pH ~ 6.7 as a function of added NaCl are shown in Figure 5a, and the corresponding changes in the particle sizes are reported in Figure 5b. Addition

of salts to colloidal dispersions typically leads to screening of electrostatic interactions between the particles.[53] The zeta potential of native Indulin AT nanoparticles at pH 6 and 300 mM NaCl (Debye length < 0.02 nm) was - 12 ± 1.3 mV, but no particle aggregation was observed (Figure 5b). The long-term stability of the nanoparticles at 300 mM NaCl was confirmed by re-measuring the particle diameters after 36 months with no aggregation or significant change in particle size and polydispersity (Figure S8a,b). However, particle aggregation was observed upon increasing the dispersion salinity to 500 mM NaCl. Similar to native nanoparticles, the long-term stability of PDAC-coated particles at 20 mM NaCl was confirmed after 36 months (Figure S8c,d). In contrast to the native nanoparticles, PDAC-coated particles showed signs of aggregation at 50 mM of NaCl, as indicated by the increase in particle size (Figure 5b). The zeta potential of these PDAC-coated particles in 50 mM electrolyte was determined +18.5 ± 0.4 mV. This partial aggregation of the nanoparticles can be attributed to the screening of charges on the particle surfaces,[54] and collapse of the PDAC polyelectrolyte on the nanoparticles' surfaces upon increasing the ionic strength.[55]

**Discussion of Indulin AT Nanoparticles Data**. The Indulin AT nanoparticles exhibited temperature-dependent growth upon pH drop in ethylene glycol solution. The protonation of the lignin molecules after inducing a pH drop in ethylene glycol may decrease their net negative charge and solubility, leading to supersaturation. An increase in the dispersion temperature increases the diffusion coefficient,[47] and increases the solubility of the lignin, both of which may result into the observed accelerated particle growth. When the particles are transferred from ethylene glycol into aqueous solution, the solubility of the Indulin AT molecules will decrease, suppressing the molecular redistribution between the particles and leading to their long-term stabilization.

The adsorption of PDAC onto the surface of Indulin AT nanoparticles resulted in charge reversal from negative to positive. In addition, the PDAC coating increased the particles' stability against dissolution at elevated pH. PDAC is a high-charge density cationic polyelectrolyte that interacts with polyanions to form polyelectrolyte complexes. The stability of these complexes is dependent on the interplay of electrostatic, van der Waals, and hydrophobic interactions.[55] The increase in the stability of Indulin AT nanoparticles with PDAC surface coating can be attributed to the formation of a stable shell of polyelectrolyte-lignin complex around the particles restricting the lignin dissolution at elevated pH.

Charged particles in aqueous dispersions are stabilized by repulsive electrostatic double-layer interactions, where the overlap of diffusive ion layers generates strong repulsion.[56] This repulsion could be readily screened with addition of salt, resulting into particle aggregation.[57] In our case, native Indulin AT nanoparticles did not show signs of aggregation at elevated dispersion salinities, indicating that the repulsive electrostatic interactions alone are not the primary stabilization mechanism. We speculate that the stability of these nanoparticles at low surface potential could originate from several factors such as steric

repulsions between the Indulin AT polymer chains on the surface of the particles[31], physical inhomogeneities of the particles' surface (roughness)[58], and other sources of short-range repulsion. Further studies would be necessary to elucidate the origin of the stabilization mechanism at elevated salinities.

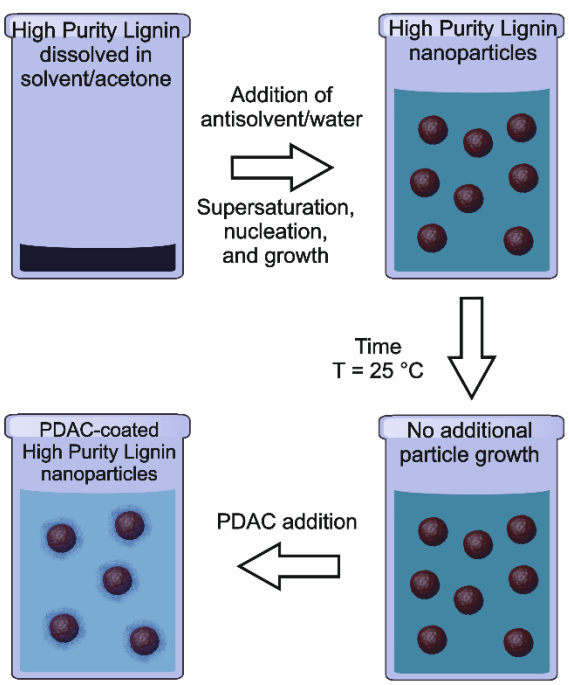


**Figure 6**. Schematics of the method for synthesis of High Purity Lignin nanoparticles. HPL is dissolved in acetone, and the particles are precipitated by addition of water, acting as antisolvent. Subsequent PDAC addition results in PDAC-coated HPL nanoparticles with positive surface charge.

**High Purity Lignin Nanoparticles - Synthesis of High Purity Lignin Nanoparticles**. The second type of investigated nanoparticles were synthesized from High Purity Lignin (HPL). The Indulin AT nanoparticles presented in the previous section are partly hydrophilic, which may limit their loading capacity for hydrophobic actives. In order to overcome this limitation, we synthesized a new type of nanocarriers using Organosolv lignin, which is more hydrophobic.[59] Since HPL is soluble in acetone, which is miscible with water (non-solvent for HPL), we can achieve controllable flash precipitation of nanoparticles by rapid dilution of HPL-acetone solution in water (Figure 6).[60] These HPL nanoparticles exhibited colloidal stability after the addition of water as antisolvent, without the need to remove the residual acetone. The main parameters governing the size of the HPL nanoparticles are (i) the dilution rate with antisolvent, and (ii) initial HPL concentration in the solvent stock solution, which are investigated further in the following section.

**Growth Parameters of High Purity Lignin Nanoparticles**. The rate of antisolvent (water) dilution was varied in the range 1-1100 mL/min (Experimental Section). The change in particle diameter upon changing the rate of water addition to HPL in acetone is shown in Figure 7a. We observed a decrease in the particle size with increasing antisolvent dilution rate. The size of the nanoparticles did not change at dilution rates > 400 mL/min, indicating that beyond this threshold value of rapid mixing, the number of nuclei formed has reached its maximum.

The equilibrium size of the nanoparticle is dependent on the initial HPL concentration in acetone. We investigated the change in particle size in the HPL concentration range from 0.1 to 3.2 wt % at a constant antisolvent dilution rate of 1100 mL/min. Figure 7b shows a monotonic increase in the nanoparticle size with increasing HPL concentration. Here we propose a geometrical model (based on lignin mass balance) to account for this increase. The basic assumptions of the model are (a) a constant number of initial nuclei (*N*) with diameter $D_0$ (= 45 nm), which are formed at the corresponding $w_0$ = 0.2 wt %, the lowest HPL loading at which stable particles could be synthesized, and (b) any further increase in the lignin bulk concentration leads to particle growth. The diameter of the lignin nanoparticles is dependent on the amount of lignin in the dispersion as $N \times D_0^3 \propto w_0$. At constant *N*, the particle diameter ($D_{HPL}$) at a given bulk lignin concentration ($w$) can be estimated by the following equation

$$D_{HPL}\,[nm] = D_0 \sqrt[3]{\frac{w}{w_0}} \qquad (2)$$

where $D_0$ is the diameter of the nuclei formed at this $w_0$. We observed good correlation between the measured data and the mass balance model, without using any fitting parameter, up to concentrations of $w$ = 1.25 wt % of lignin (Figure 7b). Further details of the data fitting are provided in supporting information (equations S1 and S2). The observed deviations of the geometric model from the experiments can be attributed to the increase in the relative population of the nuclei with increasing lignin bulk concentration. This model ignores the thermodynamic and kinetic effects of particle nucleation and growth. In principle, the number of nuclei (*N*) formed at any fixed time scales linearly with supersaturation ratio *c*/*c**, i.e. $N \propto c/c^*$, where *c* is the concentration of lignin in bulk liquid, and $c^*$ is equilibrium lignin concentration in supersaturated state.[45] However, we believe that this weak linear dependence of *N* on *c* is further suppressed by the high mixing rate used in the experiments. Hence we observe deviations from the model in the measured particle sizes only at high solute concentrations ($w$ > 1.25 wt %). Particles with diameters up to 250 nm can be synthesized by increasing the initial HPL bulk concentration beyond 3.2 wt % (Figure S7).

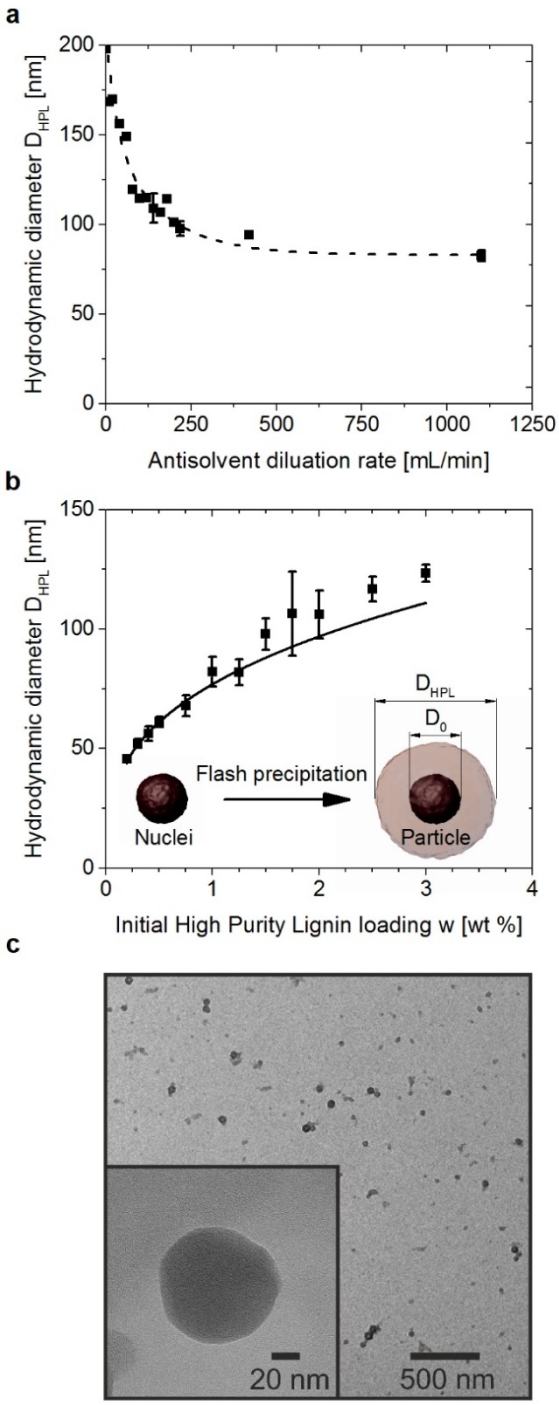


**Figure 7.** Characterization of High Purity Lignin nanoparticles. **a,** Size control by dilution rate - diameter of nanoparticles as a function of water antisolvent dilution rate at constant HPL loading during the flash precipitation. The diameter of the nanoparticles increases with increasing antisolvent addition rate. **b,** Size control as a function of initial HPL bulk concentration at constant antisolvent addition rate of 1100 mL/min. The data points are fitted using equation 2 of the lignin mass-balance model. The diameter of the nanoparticles increases with increasing HPL loading.

**c,** TEM micrograph of as-synthesized HPL nanoparticles in the size range of 60 nm to 80 nm. Error bars in **a** and **b** represent the standard deviation of the corresponding experimental values.

We visualized the High Purity Lignin nanoparticles with Transmission Electron Microscopy (TEM). The TEM images of as-synthesized HPL nanoparticles shown in Figure 7c indicate the presence of spheroidal particles with diameters below 100 nm. The particle size distribution may vary due to material properties such as a broad molecular weight distribution of the biopolymer and fluid dynamic mechanism related phenomena including locally inhomogeneous mixing regimes in batch flash precipitation.

**Properties of HPL Nanoparticles**. Similarly to the case of Indulin AT, pH and ionic strength strongly influenced the dispersion stability of HPL nanoparticles. The variation of the diameters and zeta potentials of the HPL lignin nanoparticles with increasing pH are shown in Figure 8a. The nanoparticle dispersions were stable in a broad pH range from 3.2 to 8.5, with a diameter of ~ 80 nm and zeta potential of ~ -45 mV. At pH < 3.2, the magnitude of the surface charge of the nanoparticles decreased significantly, which resulted in aggregation (Figure 8a inset). This highlights the dominant role of the electrostatic repulsion in the stabilization of the dispersion. However, at pH > 8.5 the particle size decreased to 50 nm. The decrease in particle size can be attributed to the onset of particle dissolution, where the complete dissolution occurred at pH > 12.0. The dissolution of the HPL lignin in basic solution resulted in significantly darker solution compared with the nanoparticle dispersions at pH < 8.5 (Figure 8a inset).

The pH stability study indicated that the primary interaction leading to the stabilization of the HPL particles is electrostatic double layer repulsion. In order to investigate this further, we added increasing amounts of NaCl to the nanoparticle dispersions to screen the electrostatic interactions. The size and zeta potential of HPL nanoparticles as a function of NaCl added are plotted Figure 8b. The nanoparticle dispersions were stable at ionic strength up to 70 mM. A two-and-a-half fold increase in particle size at 150 mM (Debye length < 0.03 nm) indicates the onset of particle aggregation as the zeta potential dropped below -20 mV (-18.1 mV) due to the screening of charges on the particles' surfaces.

A precise control over the surface properties of these nanoparticles is the key to their binding with charged targeted surfaces, like bacterial cell walls. As in the case of Indulin AT lignin, we selectively adsorbed positively charged PDAC onto negatively charged binding sites on the HPL nanoparticles, leading to reversal of the particles' charge from negative to positive. The change in zeta potential as a function of amount of PDAC added is shown in Figure 8c. Corresponding size measurements were performed to validate the colloidal stabilities of the dispersions after PDAC addition. At PDAC to HPL weight ratios of 0.01 to 0.03, a multifold particle size increase, indicating aggregation, was observed. Charge neutrality of

PDAC-coated HPL nanoparticles, marked by aggregation, was determined at pH 6 at a PDAC to HPL wt % ratio of 0.02. Stable dispersions of PDAC-coated nanoparticles with positive zeta potentials above +20 mV could be formed at PDAC to HPL wt % ratios of 0.06 or higher. The native and PDAC-coated HPL nanoparticles were found to be highly stable in aqueous dispersions with no change in the particle size after 36 months (see Figure S9).

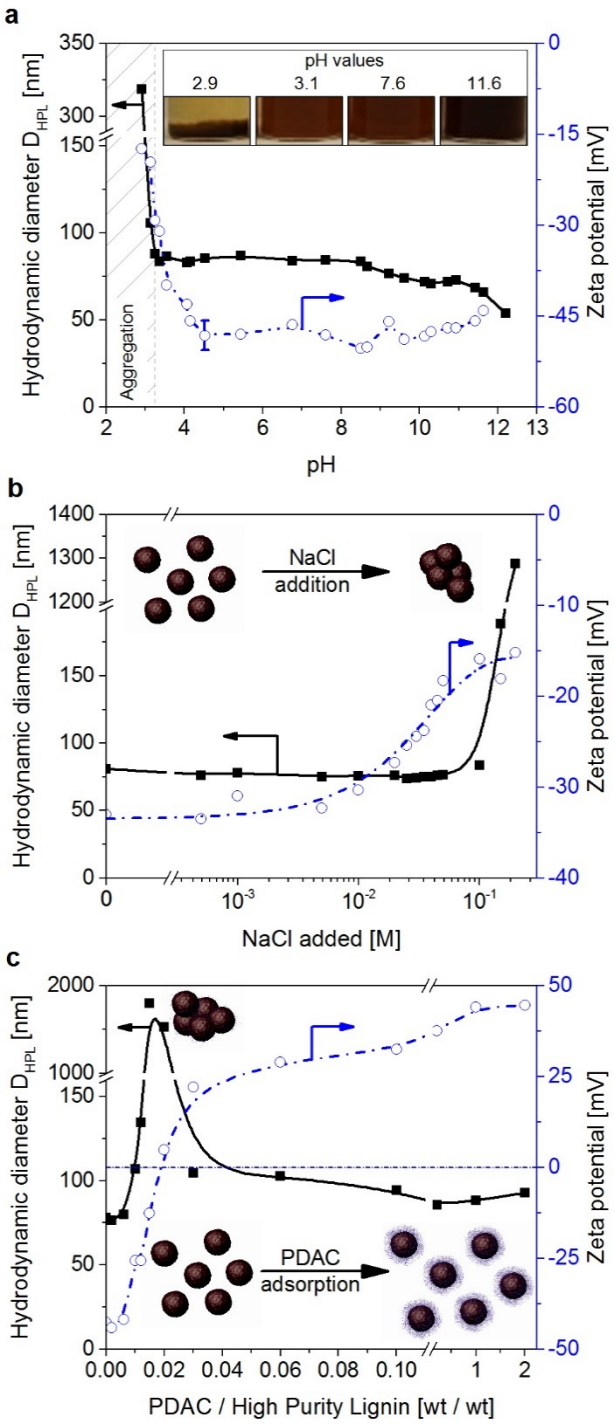

**Figure 8.** Properties of High Purity Lignin nanoparticles. **a,** pH stability of HPL nanoparticles - diameter and zeta potential as a function of dispersion pH. Aggregation is observed for pH < 3.2. The nanoparticles are stable in the pH range of 3.5 to 8. The physical appearance of the samples from pH 2.9 to 11.6 is shown in the inset. **b,** HPL nanoparticle stability at increased ionic strength - diameter and zeta potential as a function of NaCl added. The nanoparticles exhibit dispersion stability up to 70 mM. **c,** Surface charge modification from negative to positive - diameter and zeta potential of nanoparticles as a function of PDAC added. PDAC to HPL weight ratios from 0.01 to 0.03 result in aggregation of nanoparticles. PDAC to HPL weight ratios of 0.06 or higher result in stable dispersions of PDAC-coated nanoparticles with positive surface charges.

**Discussion of High Purity Lignin Nanoparticles**. The general approach of flash-precipitation was successfully used for nanoparticle formation from Kraft and Organosolv lignin. In the latter case, the short supersaturation time in the antisolvent flash-precipitation resulted in rapid particle growth depleting the solution from dissolved polymer.[47] Unlike the growth of Indulin AT nanoparticles in ethylene glycol, no further increase in particle size was observed for HPL nanoparticles after synthesis. The predominant shape of HPL nanoparticles was spheroidal (TEM, Figure 7c), similar in shape of particles from acetylated[34] and Softwood Kraft lignin,[35] whereas the Indulin AT nanoparticles (TEM, Figure S10) were irregularly shaped.[31,39] The non-spherical shape of Indulin AT nanoparticles increases the available surface area compared to spheroidal structures for adsorption of active ingredients increasing the loading capacity of the carrier.[39] The origin of this non-spherical shape for Indulin AT nanoparticles, and the spheroidal shape of HPL, may lie in the physiochemical properties of the lignin precursor used, which may vary significantly depending upon the process used for isolating the lignin. Further studies would be necessary to determine the influence of precursor on particle shape, which are beyond the focus of the present work.

As with Indulin AT, the HPL nanoparticles exhibit pH stability in a broad range. In the acidic pH regime, native HPL nanoparticles showed aggregation at a higher pH value compared to Indulin AT. The difference may be attributed to strongly deprotonating functional groups, such as thiol and carboxylic groups, present in Indulin AT, but not in HPL (see Table 1). Based on the percentages of functional groups present in Indulin AT and HPL, we infer that Indulin AT provides more sufficient negative charges for electrostatic stabilization at low pH than HPL. Both types of nanoparticles dissolve at strongly basic pH, which follows general pH-dependent dissolution properties of lignin.[59] Different from the lignin particles without PDAC coating reported by Lievonen et al,[35] native HPL and IAT particles do not have an isoelectric point at low pH or show a non-dissolution stability at pH 12.

The colloidal stabilization mechanism of native HPL nanoparticles differs from Indulin AT. The native HPL nanoparticles exhibit only moderate ionic strength stability, with particle aggregation > 100 mM NaCl. The relatively low ionic strength at which colloidal destabilization was observed indicates a purely electrostatic stabilization of the particles. Because of the high hydrophobicity of the HPL nanoparticles, we

believe that they may be well suited as potential biodegradable carriers to enhance the activity of hydrophobic bioactive compounds, such as antifungal azoles, allylamines and others.

## 4. CONCLUSIONS

Lignin nanoparticles could serve as a new class of biodegradable colloids with tunable surface properties. In this study, we used two types of lignin precursor, namely Kraft (Indulin AT) and Organosolv (HPL). The nanoparticles from both types of lignin precursors were formed by supersaturation, nucleation, and particle growth induced with flash-precipitation methods. Our studies indicate that HPL nanoparticles are only electrostatically stabilized, while the stabilization mechanism of Kraft lignin (Indulin AT) nanoparticles is more complex with additional hydration or steric interactions facilitating the particle stability at elevated salinities and low zeta potentials. Both particle systems are stable within a broad pH range from moderate acidic beyond the physiological pH, covering a wide application spectrum. While the particles dissolve in highly basic pH medium, this behavior would not interfere with large scale applications in the environment, where water is at slightly acidic pH. The amphiphilic nature of Indulin AT particles renders them suitable for functionalization with cationic actives such as antimicrobial silver ions. The HPL particles are strongly hydrophobic and extend the range of active ingredients to organic actives such as antifungal agrochemicals. We showed that the coating of the particles with PDAC allows to modify the surface charge of both nanoparticles, which in turn influences their interaction with charged targeted substrates. While PDAC is a basic charged polyelectrolyte, more complex coatings from compounds such as polysaccharides may impart in the future additional properties and another level of biological functionality.

The results in this report can enable the formulation of a nanoparticle platform for the next-generation of sustainable delivery nanovehicles for antimicrobials, fungicides, pesticides, and drugs. We demonstrated that one can make particles with readily scalable methods in a broad range of sizes, core hydrophobicities and surface charges depending on the fabrication process parameters, and material choices. This may allow controlling both the core affinity to the actives that will be delivered as well as the nanoparticle targeting and adhesion properties. The “benign-by-design” nanomaterial design principles developed here can be applied in the synthesis of numerous types of nanoparticulate carriers for actives from other biopolymers.

## ASSOCIATED CONTENT

### Supporting Information

Dynamic light scattering data, UV spectra, data on the kinetics of nanoparticle synthesis, multi-year stability evaluation, mass balance equations for HPL nanoparticle synthesis, TEM image of Indulin AT lignin nanoparticles, and data on properties of High Purity Lignin. This material is available free of charge at http://pubs.acs.org

## AUTHOR INFORMATION

**Corresponding Author**

*E-mail: odvelev@ncsu.edu. Phone (+1) 919-513-4318.

## ACKNOWLEGEMENTS

The authors acknowledge the funding from US Environmental Protection Agency via Pathfinder Innovation Projects grant, US National Science Foundation Tringle Center for Programmable Soft Matter (DMR-1121107) and North Carolina State University. APR and HBA thank BENANOVA Inc. for sponsorship. APR thanks the Lemelson Foundation and the Lemelson-MIT Program for support. VNP thanks for the financial support of European Cooperation in COST Action CM1101. SDS thanks for the financial support of European Cooperation in in COST Action MP1105, MP1106, and MP1305, as well the EU Project FP7-REGPOT-2011-1, "Beyond Everest". We thank A. K. Sarkar for assistance with preliminary studies and R. Garcia for Transmission Electron Microscopy analysis at North Carolina State University.

## REFERENCES

1. Khin, M. M.; Nair, A. S.; Babu, V. J.; Murugan, R.; Ramakrishna, S., A review on nanomaterials for environmental remediation. *Energy Environ. Sci.* **2012,** *5* (8), 8075-8109.
2. Ditta, A.; Arshad, M.; Ibrahim, M., Nanoparticles in sustainable agricultural crop production: Applications and perspectives. In *Nanotechnology and Plant Sciences*, Siddiqui, M. H.; Al-Whaibi, M. H.; Mohammad, F., Eds. Springer International Publishing: 2015; pp 55-75.
3. Rai, M.; Yadav, A.; Gade, A., Silver nanoparticles as a new generation of antimicrobials. *Biotechnol. Adv.* **2009,** *27* (1), 76-83.
4. Bystrzejewska-Piotrowska, G.; Golimowski, J.; Urban, P. L., Nanoparticles: their potential toxicity, waste and environmental management. *Waste Manage.* **2009,** *29* (9), 2587-2595.
5. Walser, T.; Limbach, L. K.; Brogioli, R.; Erismann, E.; Flamigni, L.; Hattendorf, B.; Juchli, M.; Krumeich, F.; Ludwig, C.; Prikopsky, K.; Rossier, M.; Saner, D.; Sigg, A.; Hellweg, S.; Gunther, D.; Stark, W. J., Persistence of engineered nanoparticles in a municipal solid-waste incineration plant. *Nat. Nanotechnol.* **2012,** *7* (8), 520-524.
6. Jeong, E.; Im, W.-T.; Kim, D.-H.; Kim, M.-S.; Kang, S.; Shin, H.-S.; Chae, S.-R., Different susceptibilities of bacterial community to silver nanoparticles in wastewater treatment systems. *J. Environ. Sci. Health., Part A* **2014,** *49* (6), 685-693.
7. Mitrano, D. M.; Rimmele, E.; Wichser, A.; Erni, R.; Height, M.; Nowack, B., Presence of nanoparticles in wash water from conventional silver and nano-silver textiles. *ACS Nano* **2014,** *8* (7), 7208-7219.
8. António, D. C.; Cascio, C.; Jakšić, Ž.; Jurašin, D.; Lyons, D. M.; Nogueira, A. J. A.; Rossi, F.; Calzolai, L., Assessing silver nanoparticles behaviour in artificial seawater by mean of AF4 and spICP-MS. *Mar. Environ. Res.* **2015,** *111*, 162-169.
9. Stern, S. T.; McNeil, S. E., Nanotechnology safety concerns revisited. *Toxicol. Sci.* **2008,** *101* (1), 4-21.
10. Anastas, P.; Eghbali, N., Green chemistry: Principles and practice. *Chem. Soc. Rev.* **2010,** *39* (1), 301-312.
11. Duan, H.; Wang, D.; Li, Y., Green chemistry for nanoparticle synthesis. *Chem. Soc. Rev.* **2015,** (44), 5778-5792.

12. Gilbertson, L. M.; Zimmerman, J. B.; Plata, D. L.; Hutchison, J. E.; Anastas, P. T., Designing nanomaterials to maximize performance and minimize undesirable implications guided by the Principles of Green Chemistry. *Chem. Soc. Rev.* **2015,** (44), 5758-5777.
13. Aouada, F.; de Moura, M., Nanotechnology applied in agriculture: Controlled release of agrochemicals. In *Nanotechnologies in Food and Agriculture*, Rai, M.; Ribeiro, C.; Mattoso, L.; Duran, N., Eds. Springer International Publishing: 2015; pp 103-118.
14. Wang, J.; Deng, Y.; Qian, Y.; Qiu, X.; Ren, Y.; Yang, D., Reduction of lignin color via one-step UV irradiation. *Green Chemistry* **2016,** (18), 695-699.
15. Lora, J. H.; Glasser, W. G., Recent industrial applications of lignin: A sustainable alternative to nonrenewable materials. *J. Polym. Environ.* **2002,** *10* (1), 39-48.
16. Habibi, Y.; Lucia, L. A.; Rojas, O. J., Cellulose nanocrystals: Chemistry, self-assembly, and applications. *Chem. Rev.* **2010,** *110* (6), 3479-3500.
17. Norgren, M.; Edlund, H., Lignin: Recent advances and emerging applications. *Curr. Opin. Colloid Interface Sci.* **2014,** *19* (5), 409-416.
18. Ruiz-Dueñas, F. J.; Martínez, Á. T., Microbial degradation of lignin: How a bulky recalcitrant polymer is efficiently recycled in nature and how we can take advantage of this. *Microb. Biotechnol.* **2009,** *2* (2), 164-177.
19. Jiang, S.; Kai, D.; Dou, Q. Q.; Loh, X. J., Multi-arm carriers composed of an antioxidant lignin core and poly (glycidyl methacrylate-co-poly (ethylene glycol) methacrylate) derivative arms for highly efficient gene delivery. *J. Mater. Chem. B* **2015,** *3* (34), 6897-6904.
20. Ugartondo, V.; Mitjans, M.; Vinardell, M. P., Comparative antioxidant and cytotoxic effects of lignins from different sources. *Bioresour. Technol.* **2008,** *99* (14), 6683-6687.
21. Qian, Y.; Qiu, X.; Zhu, S., Lignin: a nature-inspired sun blocker for broad-spectrum sunscreens. *Green Chemistry* **2015,** *17* (1), 320-324.
22. Peretti, S. W.; Barton, R.; Mendonca, R., Lignin as Feedstock for Fibers and Chemicals. In *Commercializing Biobased Products: Opportunities, Challenges, Benefits, and Risks*, Royal Society of Chemistry: 2015; pp 132-165.
23. Tuomela, M.; Vikman, M.; Hatakka, A.; Itävaara, M., Biodegradation of lignin in a compost environment: A review. *Bioresour. Technol.* **2000,** *72* (2), 169-183.
24. Bugg, T. D. H.; Ahmad, M.; Hardiman, E. M.; Rahmanpour, R., Pathways for degradation of lignin in bacteria and fungi. *Nat. Prod. Rep.* **2011,** *28* (12), 1883-1896.
25. Sarkanen, K. V.; Ludwig, C. H., *Lignins: Occurrence, formation, structure and reactions*. John Wiley & Sons: 1971.
26. Chakar, F. S.; Ragauskas, A. J., Review of current and future softwood kraft lignin process chemistry. *Ind. Crops Prod.* **2004,** *20* (2), 131-141.
27. Calvo-Flores, F. G.; Dobado, J. A., Lignin as renewable raw material. *ChemSusChem* **2010,** *3* (11), 1227-1235.
28. Duval, A.; Lawoko, M., A review on lignin-based polymeric, micro- and nano-structured materials. *React. Funct. Polym.* **2014,** *85* (0), 78-96.
29. §205.601 - Synthetic substances allowed for use in organic crop production. In *Code of Federal Regulations: Titel 7, Subtitle B, Chapter 1, Subchapter M, Part 205, Subpart G.*, GPO, Ed. U.S. Government Publishing Office: 2015.
30. Alloway, B., Micronutrients and crop production: An introduction. In *Micronutrient Deficiencies in Global Crop Production*, Alloway, B., Ed. Springer Netherlands: 2008; pp 1-39.

31. Frangville, C.; Rutkevičius, M.; Richter, A. P.; Velev, O. D.; Stoyanov, S. D.; Paunov, V. N., Fabrication of environmentally biodegradable lignin nanoparticles. *ChemPhysChem* **2012,** *13* (18), 4235-4243.
32. Wege, H. A.; Kim, S.; Paunov, V. N.; Zhong, Q.; Velev, O. D., Long-term stabilization of foams and emulsions with in-situ formed microparticles from hydrophobic cellulose. *Langmuir* **2008,** *24* (17), 9245-9253.
33. Myint, A. A.; Lee, H. W.; Seo, B.; Son, W.-S.; Yoon, J.; Yoon, T. J.; Park, H. J.; Yu, J.; Yoon, J.; Lee, Y.-W., One pot synthesis of environmentally friendly lignin nanoparticles with compressed liquid carbon dioxide as an antisolvent. *Green Chemistry* **2015**.
34. Qian, Y.; Deng, Y.; Qiu, X.; Li, H.; Yang, D., Formation of uniform colloidal spheres from lignin, a renewable resource recovered from pulping spent liquor. *Green Chemistry* **2014,** *16* (4), 2156-2163.
35. Lievonen, M.; Valle-Delgado, J. J.; Mattinen, M.-L.; Hult, E.-L.; Lintinen, K.; Kostiainen, M. A.; Paananen, A.; Szilvay, G. R.; Setala, H.; Osterberg, M., A simple process for lignin nanoparticle preparation. *Green Chemistry* **2015,** (18), 1416-1422.
36. Gilca, I. A.; Popa, V. I.; Crestini, C., Obtaining lignin nanoparticles by sonication. *Ultrason. Sonochem.* **2015,** *23*, 369-375.
37. Nypelö, T. E.; Carrillo, C. A.; Rojas, O. J., Lignin supracolloids synthesized from (W/O) microemulsions: Use in the interfacial stabilization of Pickering systems and organic carriers for silver metal. *Soft Matter* **2015,** *11* (10), 2046-2054.
38. Lam, S.; Velikov, K. P.; Velev, O. D., Pickering stabilization of foams and emulsions with particles of biological origin. *Curr. Opin. Colloid Interface Sci.* **2014,** *19* (5), 490-500.
39. Richter, A. P.; Brown, J. S.; Bharti, B.; Wang, A.; Gangwal, S.; Houck, K.; Cohen Hubal, E. A.; Paunov, V. N.; Stoyanov, S. D.; Velev, O. D., An environmentally benign antimicrobial nanoparticle based on a silver-infused lignin core. *Nat. Nanotechnol.* **2015,** *10* (9), 817-823.
40. Johnson, B. K.; Prud'homme, R. K., Chemical processing and micromixing in confined impinging jets. *AIChE Journal* **2003,** *49* (9), 2264-2282.
41. Liptak, M. D.; Gross, K. C.; Seybold, P. G.; Feldgus, S.; Shields, G. C., Absolute pKa determinations for substituted phenols. *J. Am. Chem. Soc.* **2002,** *124* (22), 6421-6427.
42. Smith, M. B.; March, J., *March's advanced organic chemistry: Reactions, mechanisms, and structure*. John Wiley & Sons, Inc.: Hoboken, 2007.
43. Harris, D., *Quantitative chemical analysis*. 8 ed.; W. H. Freeman and Company: New York, 2010.
44. Yang, W.; Kenny, J. M.; Puglia, D., Structure and properties of biodegradable wheat gluten bionanocomposites containing lignin nanoparticles. *Ind. Crops Prod.* **2015,** *74*, 348-356.
45. Thanh, N. T. K.; Maclean, N.; Mahiddine, S., Mechanisms of nucleation and growth of nanoparticles in solution. *Chem. Rev.* **2014,** *114* (15), 7610-7630.
46. Ribeiro, C.; Lee, E. J. H.; Longo, E.; Leite, E. R., A kinetic model to describe nanocrystal growth by the oriented attachment mechanism. *ChemPhysChem* **2005,** *6* (4), 690-696.
47. Viswanatha, R.; Sarma, D. D., Growth of Nanocrystals in Solution. In *Nanomaterials Chemistry*, Wiley-VCH Verlag GmbH & Co. KGaA: 2007; pp 139-170.
48. Woehl, T. J.; Evans, J. E.; Arslan, I.; Ristenpart, W. D.; Browning, N. D., Direct in situ determination of the mechanisms controlling nanoparticle nucleation and growth. *ACS Nano* **2012,** *6* (10), 8599-8610.
49. Pesika, N. S.; Hu, Z.; Stebe, K. J.; Searson, P. C., Quenching of growth of ZnO nanoparticles by adsorption of octanethiol. *J. Phys. Chem. B* **2002,** *106* (28), 6985-6990.

50. Einstein, A., *Investigations on the theory of the Brownian movement*. Courier Corporation: 1956.
51. Norgren, M.; Lindström, B., Dissociation of phenolic groups in kraft lignin at elevated temperatures. *Holzforschung* **2000,** *54* (5), 519-527.
52. Bauer, D.; Buchhammer, H.; Fuchs, A.; Jaeger, W.; Killmann, E.; Lunkwitz, K.; Rehmet, R.; Schwarz, S., Stability of colloidal silica, sikron and polystyrene latex influenced by the adsorption of polycations of different charge density. *Colloids and Surfaces A: Physicochemical and Engineering Aspects* **1999,** *156* (1–3), 291-305.
53. Bharti, B.; Meissner, J.; Klapp, S. H. L.; Findenegg, G. H., Bridging interactions of proteins with silica nanoparticles: The influence of pH, ionic strength and protein concentration. *Soft Matter* **2014,** *10* (5), 718-728.
54. v. Klitzing, R., Internal structure of polyelectrolyte multilayer assemblies. *Phys. Chem. Chem. Phys.* **2006,** *8* (43), 5012-5033.
55. Zhang, Y.; Yildirim, E.; Antila, H. S.; Valenzuela, L. D.; Sammalkorpi, M.; Lutkenhaus, J. L., The influence of ionic strength and mixing ratio on the colloidal stability of PDAC/PSS polyelectrolyte complexes. *Soft Matter* **2015,** *11* (37), 7392-401.
56. Hierrezuelo, J.; Sadeghpour, A.; Szilagyi, I.; Vaccaro, A.; Borkovec, M., Electrostatic stabilization of charged colloidal particles with adsorbed polyelectrolytes of opposite charge. *Langmuir* **2010,** *26* (19), 15109-15111.
57. Israelachvili, J. N., *Intermolecular and surface forces: Revised third edition*. Academic press: 2011.
58. Norgren, M.; Edlund, H.; Wågberg, L., Aggregation of lignin derivatives under alkaline conditions. Kinetics and aggregate structure. *Langmuir* **2002,** *18* (7), 2859-2865.
59. Laurichesse, S.; Avérous, L., Chemical modification of lignins: Towards biobased polymers. *Prog. Polym. Sci.* **2014,** *39* (7), 1266-1290.
60. D'Addio, S. M.; Prud'homme, R. K., Controlling drug nanoparticle formation by rapid precipitation. *Adv. Drug Deliver. Rev.* **2011,** *63* (6), 417-426.